STRUCTURE, ELECTRONIC AND VIBRATIONAL STUDY OF 7-METHYL-2,3-DIHYDRO-(1,3) THIAZOLO(3,2-A)PYRIMIDIN-5-ONE BY USING DENSITY FUNCTIONAL THEORY

Bhawani Datt Joshi, Janga Bahadur Khadka and Atamram Bhatt

Journal of Institute of Science and Technology

Volume 22, Issue 2, January 2018

ISSN: 2469-9062 (print), 2467-9240 (e)

JIST, **22** (2): 1-11 (2018)

Published by:

Institute of Science and Technology

Tribhuvan University

Kirtipur, Kathmandu, Nepal

JIST 2018, 22 (2): 1-11
ISSN: 2469-9062 (p), 2467-9240 (e)

Research Article

STRUCTURE, ELECTRONIC AND VIBRATIONAL STUDY OF 7-METHYL-2,3-DIHYDRO-(1,3)THIAZOLO(3,2-A)PYRIMIDIN-5-ONE BY USING DENSITY FUNCTIONAL THEORY

Bhawani Datt Joshi[1*], Janga Bahadur Khadka[2] and Atamram Bhatt[2]
[1]Department of Physics, Siddhanath Sc, Campus, Tribhuvan University, Mahendranagar, Nepal
[2]Department of Chemistry, Siddhanath Sc, Campus, Tribhuvan University, Mahendranagar, Nepal
**Corresponding E-mail: pbdjoshi@gmail.com*

Received: *20 October, 2017;* ***Revised:*** *6 November, 2017;* ***Accepted:*** *7 December, 2017*

ABSTRACT

We have presented molecular structure and vibrational wavenumber assignments of 7-methyl-2,3-dihydro-(1,3)thiazolo(3,2-a)pyrimidin-5-one. Both *ab initio* Hartree-Fock and density functional theory employing 6-311++G(d,p) basis set have been used for the calculations. The scaled values of the calculated vibrational frequencies were used for assignments on the basis of potential energy distribution. The structure-activity relation has been interpreted by mapping molecular electrostatic potential surface. Electronic properties have been analyzed by using time dependent density functional theory (TD-DFT) for both gaseous and solvent phase. The calculated HOMO (highest occupied molecular orbital) and LUMO (lowest unoccupied molecular orbital) energy values show that the charge transfer occurs within the molecule.

Keywords: MeTPDN, DFT, Vibrational spectroscopy, HOMO and LUMO.

INTRODUCTION

In recent years, there is an urgent need to develop new antimicrobial drugs with potent activities in order to overcome the global problem of bacterial drug resistance. Heterocyclic compounds containing pyrimidine moiety are of great interest because they constitute an important class of natural and non-natural products, many of which exhibit useful biological activities and clinical applications (Bradley *et al.,* 2007; Panlilio *et al.,* 1992; Brown, 1984; Elderfield, 1957). Electron-rich nitrogen heterocycles and sulphur compounds play an important role in diverse biological activities. Thiazolo(3,2-*a*)pyrimidine derivatives are known for their broad spectrum of biological activities such as potential purine antagonists and antioxidants (El-Bayouki & Basyouni, 2010; Nagarajaiah *et al.,* 2012). They exhibit anti-inflammatory (Tozkoparan *et al.,* 1999), antihypertensive (Jeanneau-Nicolle *et al.,* 1992), antimicrobial (Jachak *et al.,* 2005), antiviral (Mohamed *et al.,* 2010), antifungal (Pan *et al.,* 2011), antitumor (Flefel *et al.,* 2007; Al-Omary *et al.,* 2012), anti-HIV (Danel *et al.,* 1998), antitubercular (Geist *et al*., 2010), calcium channel blocking (Balkan *et al.,* 1992; Cai *et al.,* 2015) etc. as their common activities.

Park *et al.* (2013), designed and synthesized the oxazolopyridine and thiazolopyridine derivatives, and biologically evaluated their inhibitory activities against monoamine oxidase B (MAO-B) with greater optimal therapeutic potential towards Parkinson's disease. Recently, Cai *et al*. (2015), reported antibacterial and antitubercular activities of some of the S-alkylated pyrimidine derivatives. Literature reveals that many synthesis and structure-activity related works on these pyrimidine derivatives had been reported, but their vibrational analysis has still not been studied. So, the aim of present study was to fully determine the molecular structure, vibrational modes and the absorption bands of 7-methyl-2,3-dihydro-(1,3)thiazolo(3,2-a)pyrimidin-5-one (MeTPDN) theoretically. Both Raman and infrared (IR) are the traditional spectroscopic methods for non-destructive characterization of substances (Chamers & Griffiths, 2002). Along with the quantum chemical studies, the equilibrium geometry, harmonic vibrational wavenumbers, molecular electrostatic potential surfaces, absolute Raman scattering

activities and IR absorption intensities have been calculated to support our wavenumber assignments using both *ab initio* Hartree-Fock (HF) and density functional theory (DFT) (Hohenberg & Kohn, 1964; Jha *et al*., 2018; Kumar *et al*., 2017; Govindarajan *et al*., 2012). Frontier levels energy gap (ΔE), dipole moments and the total energy has been obtained from the optimized geometry of the molecule. Most of the calculations have been performed for a single (or isolated) molecule in the gaseous system.

MATERIALS AND METHODS

Computational details

The DFT calculations were mainly carried out on the framework of Becke's three parameter (local, non-local, Hartree-Fock) hybrid exchange functional with Lee-yang-Parr correlation functional (B3LYP) (Casida & Chong, 1995; Casida *et al.*, 1998; Lee *et al.*, 1998). Molecular structure, vibrational frequencies and energies of the optimized structure of the molecule were calculated using Gaussian 09 (Frisch *et al.*, 2009) program package employing 6-311++G(d,p) basis set (Becke, 1993; Parr & Yang, 1989). The absolute Raman scattering and IR intensities were calculated at the same level as used for the optimization of geometry. The vibrational assignments of the normal modes were done as by Pualy's recommendation (Pulay *et al.*, 1983) along the internal coordinates employing localized symmetry using GAR2PED (Martin & Van Aslenoy, 1995). Visualization and confirmation of the calculated data were done by CHEMCRAFT program (Zhurko & Zhurko, 2005). The graphical presentation of molecular electrostatic potential surface, HOMO - LUMO, and the calculated IR and Raman spectra obtained from the Gaussian output were made using GaussView program (Frisch *et al.*, 2000).

RESULTS AND DISCUSSION

Geometry optimization

Using the standard geometric parameters, obtained from structure search data base (*https://pubchem.ncbi.*), the geometry optimization has been performed as the first task, without using any constraints. These optimized geometric parameters were used for all the other calculations. Calculated vibrational frequency and the equilibrium geometry have been determined by the energy minimization. The ground state optimized molecular structure is shown in the figure 1. The relative energies of the molecule are calculated employing *ab initio* HF functions and DFT functional. The energy calculated by DFT (-536301.423 kcal/mol) is lower showing more stability than the calculated by HF (-534115.669 kcal/mol).

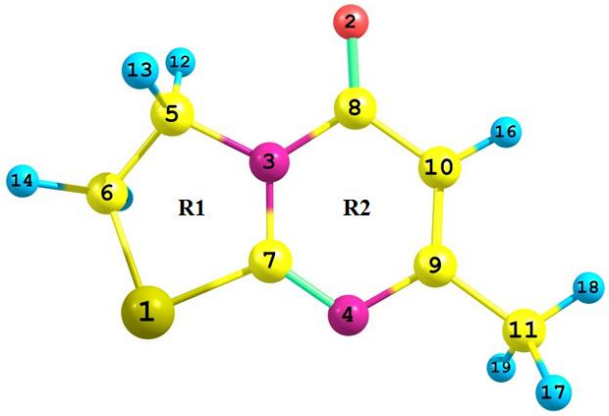

Fig. 1. Optimized structure of MeTPDN molecule.

The enthalpy difference between these two theories is 6.442 kcal/mol. The optimized parameters obtained by DFT method were very close to those obtained by the HF method. In this study, the bond lengths did not differ by more than 0.015Å except S1-C6, O2=C8, N3-C8 and N4=C7, which differed by 0.022Å, 0.0249Å, 0.0254Å and 0.0226Å, respectively. Relative to the bond lengths, both the bond angles and the dihedral angles were very similar (Srivastava *et al.*, 2010) in the two theories.

Molecular electrostatic potential surface

The molecular electrostatic potential (MEP) in a molecule at any point r(x,y,z) is a force on unit positive charge at that point due to the net charge of the system (electronic and the nuclear charge). It is given by:

$$V(r) = \sum_{A=1}^{N} \frac{Z_A}{|\vec{R}_A - \vec{r}|} - \int \frac{\rho(\vec{r'})dr}{|\vec{r'} - \vec{r}|} \qquad (1)$$

where Z_A is the charge on nucleus A located at R_A and $\rho(r')$ is the electron density. The first term is due to the nucleus and the second due to electron cloud.

The MEP is a visualization tool to understand the relative polarization of the molecules (Chidangil *et al.*, 1998). Such surfaces depict the size, shape, charge density, and site of chemical reactivity of the molecules. In the surface generated, negative electrostatic potential (shades of red color)

corresponds to an attraction of the proton by the concentrated electron density in the molecules (from lone pairs, pi-bonds, etc.) and positive electrostatic potential (shades of blue color) corresponds to repulsion of the proton by the atomic nuclei in the regions where low electron density exists and the nuclear charge is incompletely shielded. The spatial distribution and the values of the electrostatic potential are in fact largely responsible for the binding of a substrate to its receptor binding site. Different values of the electrostatic potential at the surface of a molecule appear with the different colors. The largely white or lighter color shades on the surface indicate that the molecule is mostly non-polar. The potential increases in the order red < orange < yellow < green < blue.

The electrostatic potential surface (ESP), electron density (ED), and the molecular electrostatic potential (MEP) of the molecule mapped with the output obtained by B3LYP/ 6-311++G(d,p) basis are shown in the figures 2(a-d).

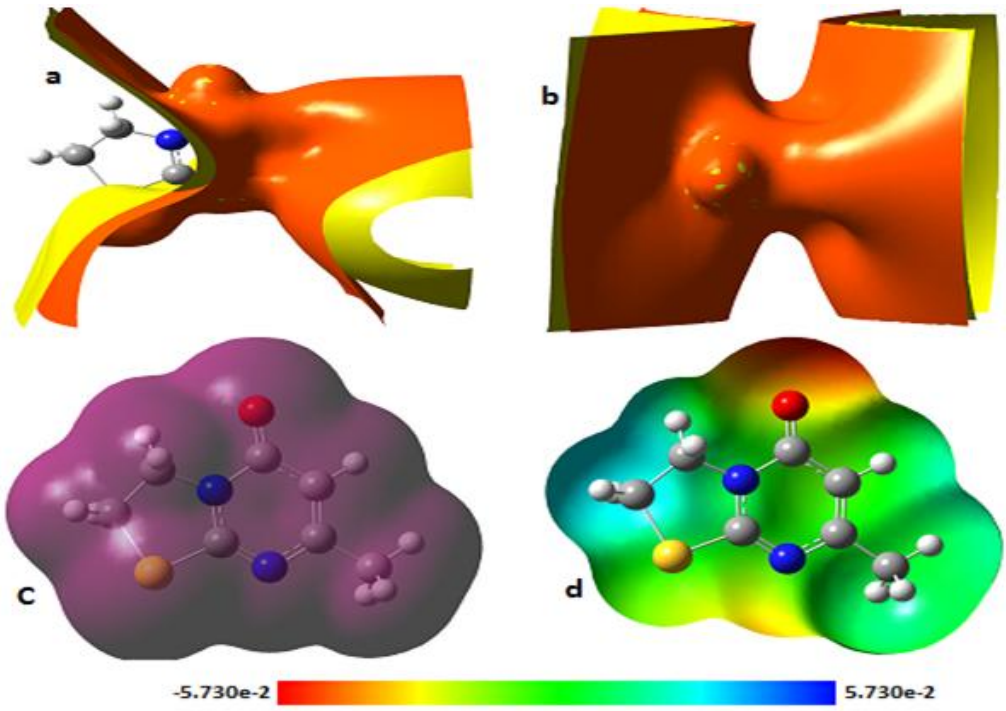

Fig. 2. Graphical representation: (a) electrostatic potential surface in-plane, (b) electrostatic potential surface perpendicular to the plane, (c) electron density, and (d) molecular electrostatic potential (mapped from -5.730e-2 to 5.730e-2).

From the figure, the highest negative potential (red region) is localized over the oxygen atom O2, as a functional group atom, of pyrimidine ring (R2). A less negative area occurs over the nitrogen atom N4 and sulphur atom S1. Similarly, the lowest potential (blue) is localized over the hydrogen atoms of the ethylene group of the thiazole ring (R1). ED mapping shows the uniform charge distribution over the molecular surface.

Electronic absorption and frontier molecular orbitals (FMOs)

In order to understand the electronic transitions in terms of energies and oscillator strengths, the time dependent density functional theory (TD-DFT)/6-31G (Petersson & Allaham, 1991) calculations were performed in the gaseous phase as well as in the solvent (EtOH) environment (integral equation formalism polarizable continuum model, IEF-PCM model) (Mishra *et al.*, 2015, Perepichka & Bryce, 2005). The theoretical UV-vis absorption spectra are shown in the figure 3. Both the frontier molecular orbitals (FMOs), HOMO and LUMO are the main orbitals taking part in the chemical reaction (Singh *et al*., 2012). Energy difference between these two orbitals is the principal factor for determining the reactivity of the system.

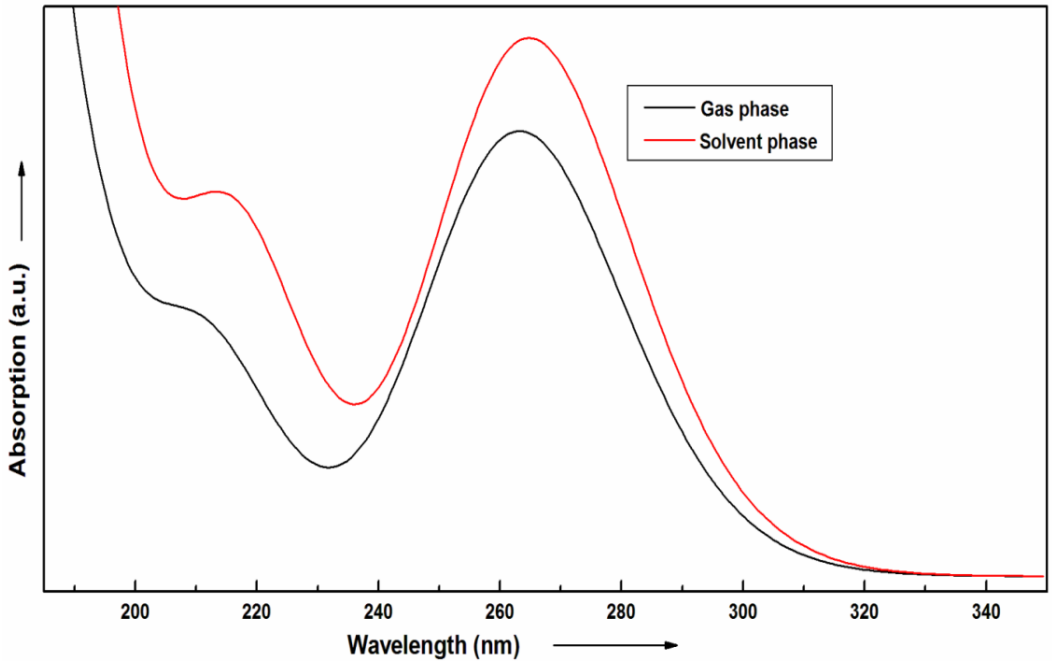

Fig. 3. Theoretical UV-vis spectra in the ranges 180-350 nm.

To understand the electronic transitions, positions of experimental absorption peaks, calculated wavelengths (λ_{max}), vertical excitation energies, oscillator strengths (f), dipole moments, and excitation transition with spectral assignments for gas and solvent environment were carried out, which is given in Table 1. From the table, the main dipole transition in gas phase occurs at 264.70 nm (H → L) with the oscillator strength 0.1246. Another strong transition is at 211.27 nm (H → L+1) with the oscillator strength 0.0708. Similarly, in solvent phase, the transitions are centered at 265.14 / 216.21 nm (H → L / H → L+1) with the oscillator strengths 0.1726 / 0.1096, respectively. It was clearly visible that both in gaseous and solvent phase in HOMO as well as in LUMO, the charge was mainly accumulated over the rings. The plots are shown in the figure 4. The main transition types occurring are n → π^* and π → π^*.

Table 1: Electronic transitions, absorption wavelength λ_{max} (nm), excitation energy (eV), oscillator strengths (f), frontier orbital energies (eV) and dipole moment, μ (Debye).

Excited states	Gas phase				Solvent (EtOH) phase			
	Transitions	λ	eV	Oscillator strength	λ	eV	Oscillator strength	Transitions
1	H → L	264.70	4.6839	0.1246	265.14	4.6761	0.1726	H → L
2	H-1 → L	256.39	4.8357	0.0203	246.68	5.0262	0.0042	H-2 → L
3	H-3 → L	247.37	5.0122	0.0036	228.76	5.4199	0.0041	H-1 → L
4	H-2 → L	227.86	5.4413	0.0073	213.95	5.7950	0.0017	H-2 → L+1
5	H → L+1	211.27	5.8685	0.0708	216.21	5.7345	0.1096	H → L+1

	E_{HOMO} (eV)	E_{LUMO} (eV)	ΔE(eV)	μ (D)
Gas	-6.370298	-1.161845	5.208452	1.9434
EtOH	-6.354760	-1.075258	5.279501	2.7012

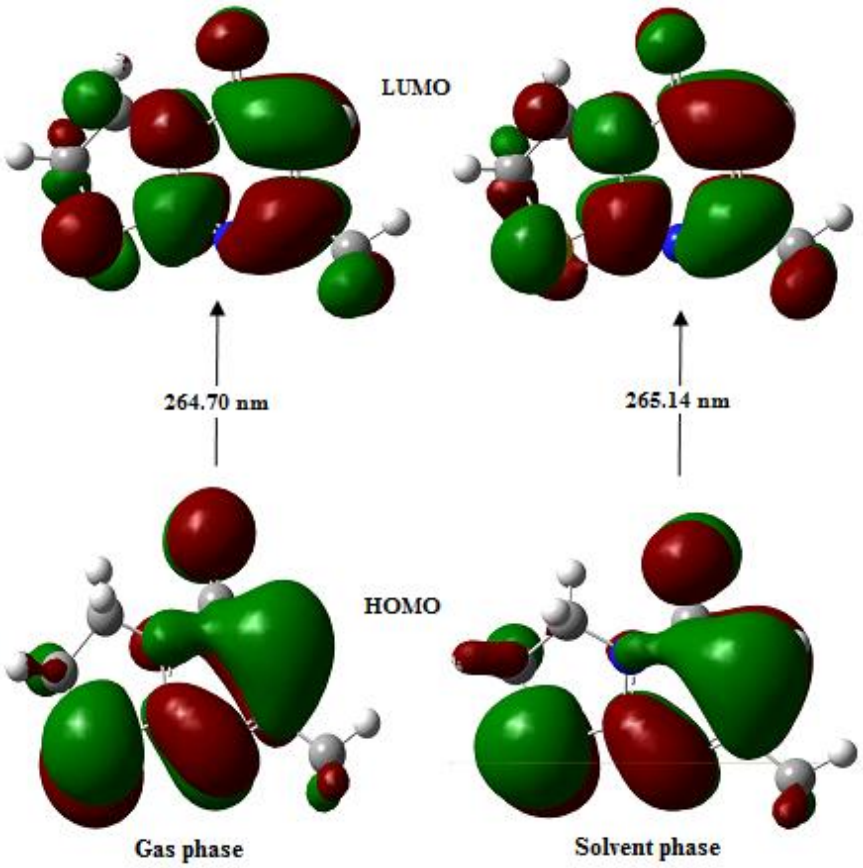

Fig. 4. HOMO-LUMO plots in the gas and solvent phases.

Vibrational spectrum

The number of atoms in this molecule is 19 and it gives 51 (3N-6, N number of atom) number of vibrations. All the vibrations are both Raman and IR active. DFT calculations yield Raman scattering amplitudes which cannot be taken directly to be the Raman intensities. The Raman scattering cross section, $\partial\sigma/\partial\Omega$, which are proportional to Raman intensity may be calculated from Raman scattering amplitude and predicted wavenumbers for each normal mode using the relationship (Guirgis *et al.*, 2003; Polavarapu, 1990):

$$\frac{\partial\sigma_j}{\partial\Omega} = \left(\frac{2^4\pi^4}{45}\right)\left(\frac{(\upsilon_0-\upsilon_j)^4}{1-exp\left[\frac{-hc\upsilon_j}{kT}\right]}\right)\left(\frac{h}{8\pi^2 c\upsilon_j}\right)S_j \qquad (2)$$

where S_j and υ_j are the scattering activities and the predicted wavenumbers, respectively of the j^{th} normal mode, υ_0 is the wavenumber of Raman excitation line and h, c and k are universal constants.

Since, the DFT and HF vibrational wavenumbers are known to be higher than the actual values due to neglect of anharmonicity effects, they were scaled down by the wavenumber linear scaling procedure (WLS) (υ_{obs} = (1.0087 - 0.0000163 $\upsilon_{calc.}$) υ_{calc} cm^{-1}) of Yoshida *et al.*, 2002. Comparison of the wavenumbers shows that the DFT methods give smaller value of the wavenumbers than the HF due to inclusion of the electron correlation in the first. The wavenumbers, intensities and the PED distributions obtained by HF and DFT methods with 6-311++G(d,p) basis set are listed in the Table 2. Calculated FT-IR and Raman spectra are shown in the figures 5 & 6. The assignments of some selected mode of vibration are discussed below:

Methyl group vibrations

Methyl (CH_3) group has several modes associated with it, such as symmetric and asymmetric stretches, bends, rocks, and torsional modes. There is a methyl group attached to the pyrimidine ring as a functional group as shown in the figure 1. The asymmetric stretching of CH_3 was predicted at 2993 and 2960 cm^{-1} with medium intensity in the Raman and weak in the IR spectra. The symmetric stretching related to this mode corresponds at 2911

cm^{-1} with strong intensity of 262 arb. units (i.e., $Å^4$/amu) in the Raman spectrum. Asymmetric and symmetric stretches were predicted at 1457 / 1451 and 1404 / 1368 cm^{-1}, respectively. The mixed rocking vibration of CH_3 was calculated at 1052 and 1038 cm^{-1}.

Table 2: Calculated FT-IR and FT-Raman wavenumbers (cm^{-1}) with their intensities.

Un scaled	Sclaled		IR Int. (km/mol)	Raman Act. ($Å^4$/amu)	Potential energy distribution %
DFT	HF	DFT			
3211	3222	3071	1.064	119.350	R2(υ(CH))(99)
3140	3150	3007	4.251	99.065	R1($υ_a(CH_2)$)(99)
3125	3139	2993	15.779	67.718	R2($υ_a(CH_3)$)(99)
3122	3121	2990	3.779	83.801	R1($υ_a(CH_2)$)(99)
3089	3096	2960	7.990	89.728	R2($υ_a(CH_3)$)(99)
3074	3086	2947	15.390	120.957	R1($υ_s(CH_2)$)(97)
3043	3069	2918	18.871	140.985	R1($υ_s(CH_2)$)(98)
3035	3043	2911	10.620	262.026	R2($υ_s(CH_3)$)(100)
1739	1867	1705	665.167	40.024	R2(υ(C=O)(66)+υ(CC)(13))
1627	1764	1598	178.614	5.162	R2(υ(C=C)(37)+υ(N=C)(22)+υ(C=O)(9))+R1(υ(NC))(6)
1553	1672	1528	406.538	66.949	R2(υ(N=C)(39)+υ(C=C)(19)+υ(NC)(7))+R1($δ_{ring}$)(6)
1514	1616	1489	40.2653	7.579	R1(δ(CH_2))(92)
1491	1588	1468	13.400	10.574	R1(δ(CH_2))(95)
1480	1570	1457	29.333	19.431	R2(δ'$_a$(CH_3))(80)
1473	1564	1451	8.594	8.633	R2($δ_a(CH_3)$(92)+ρ(CH_3)(6))
1425	1540	1404	132.119	20.906	R2($δ_s(CH_3)$(36)+υ(NC)(15)+υ(C9C11)(14))+R1(υ(NC)(8))
1408	1515	1388	43.612	3.280	R1(ω(CH_2)(34)+υ(NC)(14))+R2($δ_s(CH_3)$)(32)
1387	1482	1368	21.979	9.202	R2($δ_s(CH_3)$(24)+υ(NC)(17)+$δ_{in}$(CH)(15))+R1(ω(CH_2))(15)
1321	1424	1304	21.714	11.912	R1(ω(CH_2)(36)+γ(CH_2)(34)+υ(NC)(10))
1289	1399	1273	2.813	13.193	R1(ω(CH_2)(45)+υ(NC)(31))+R2(υ(N=C))(4)
1250	1356	1236	17.295	11.912	R1(γ(CH_2)(23)+ω(CH_2)(18)+υ(NC)(8))+R2(υ(N=C)(5))
1224	1308	1210	9.654	10.684	R2($δ_{in}$(CH)(47)+υ(C9C11)(12)+$δ_{trig}$(9))
1197	1294	1184	26.883	4.874	R1(γ(CH_2)(45)+ω(CH_2)(17)+υ(NC)(9)+υ(CC)(8)+R2($δ_{trig}$)(6)
1183	1276	1170	47.869	3.560	R1(γ(CH_2)(29)+υ(NC)(8)+δ'$_{ring}$(5))+R2(υ(NC)(18)+$δ_{trig}$(9))
1130	1198	1119	24.559	0.799	R2(υ(CC)(30)+υ(C9C11)(12)+υ(NC)(10))+R1(υ(NC))(19)
1061	1148	1052	3.119	0.549	R2(ρ(CH_3)(69)+oop(C9C11)(14)+$δ_a$(CH_3)(5)+oop(CH)(5))
1047	1130	1038	3.006	2.503	R2(ρ'(CH_3)(31)+$δ_{trig}$(12)+$δ_{in}$(CH)(7)+υ(NC)(7)+υ(C=C)(6)+ R1(ρ(CH_2))(14)
1034	1116	1025	7.680	2.712	R1(ρ(CH_2))(50)+γ(CH_2)(12)+R2(ρ'(CH_3))(20)
996	1074	988	7.185	3.228	R2(υ(NC)(27)+$δ_{trig}$(12)+ρ'(CH_3)(11))+R1(γ(CH_2)(8)+δ'$_{ring}$(7)+ ρ(CH_2)(6))
988	1046	981	1.067	1.562	R1(υ(CC))(71)+R2(υ(CC))(14)
911	976	906	9.587	6.852	R1(υ(SC)(22)+ρ(CH_2)(11))+R2(υ(NC)(17)+δ'$_a$(17)+ υ(C9C11)(12))

877	947	872	3.808	1.354	R1($\rho(CH_2)$(41)+δ'_{ring}(11)+υ(SC)(9)+υ(NC)(5))+ R2(υ(NC) (8)+υ(C9C11)(6)+δ_{trig}(5))
851	919	846	28.339	0.583	R2(oop(CH)(72)+oop(C=O)(14)+puck(7))
767	841	764	9.040	5.245	R1(υ(NC)(20)+$\rho(CH_2)$(9)+δ'_{ring}(6))+R2(puck(17)+ oop(C=O)(12)+δ_{trig}(9))
747	812	745	6.185	1.521	R2(puck(38)+oop(C=O)(28)+oop(C9C11)(6))+R1(υ(NC))(6)
686	760	685	4.141	12.191	R1(υ(SC)(70)+δ'_{ring}(12))+R1(ρ(CH2))(8)
665	737	663	0.789	0.205	R2(τ'(23)+oop(C=O)(19)+puck(19)+oop(C9C11)(8))+ τ(N3C7)(15)+R1(τ(8)+
632	682	631	3.660	2.683	R2(δ_{in}(C=O)(30)+δ'_a(15)+δ_{in}(C9C11)(13))+R1(δ'_{ring}(10)+ υ(NC)(9)+δ_{ring}(5))
577	632	577	2.832	3.061	R2(oop(C9C11)(43)+τ(26)+$\rho(CH_3)$(6))+R1(τ)(8)
571	611	570	7.826	13.523	R2(δ'_a(13)+υ(CC)(13)+δ_{in}(C=O)(11)+oop(C9C11)(10)+ υ(C9C11)(10)+δ_{trig}(8)+ τ(5))+R1(δ_{ring})(6)
537	584	537	0.145	0.353	R1(δ_{ring}(42)+δ_a(29)+υ(SC)(11)+$\rho(CH_2)$(6))
440	475	441	1.072	6.991	R2(δ_a(39)+υ(CC)(5))+R1(δ_{ring}(34)+υ(NC)(6))
428	469	429	5.397	6.381	R1(υ(SC))(46)+R2(δ'_a(24)+δ_{in}(C9C11)(13)+υ(NC)(6))
322	352	323	3.929	1.269	R2(δ_{in}(C=O)(32)+δ_{in}(C9C11)(31)+δ_a(7)+υ(NC)(6))
270	284	271	0.352	0.583	τ(N3C7)(43)+R1(τ)(39)+ R2(τ)(10)
257	277	258	5.188	1.337	R2(δ_{in}(C9C11)(38)+δ_a(5))+R1(δ_{ring}(20)+υ(SC)(7))
199	220	200	4.846	0.354	R2(τ'(53)+oop(CH)(9))+R1(τ')(20)+τ(N3C7)(9)
183	197	185	0.381	0.822	R1(τ)(49)+R2(oop(CH)(14)+puck(13)+τ'(5))
131	155	132	0.170	0.339	R2(puck(30)+τ(11)+oop(C9C11)(9)+oop(CH)(6))+ R1(τ')(24)+τ(N3C7)(11)
127	144	128	0.225	0.286	τ(C9C11)(70)+R2(τ')(13)
98	106	99	9.248	0.070	R2(τ(38)+puck(5))+τ(N3C7)(29)+R1(τ')(22)

υ, stretching, δ, deformation, δ_{in}, in-plane deformation, oop, out-of-plane deformation, w, wagging, ρ , rocking, γ, twisting and τ, torsion.

Thiazole ring (R1) vibrations

The methylene (CH_2) groups are characterized by six fundamental modes of vibration. Out of them symmetric and asymmetric stretch, bending and rocking modes belong to polarized in-plane vibration. Similarly, wagging and twisting modes belong to the depolarized out-of-plane vibration (Joshi *et al.*, 2011). The asymmetric CH_2 stretching vibrations are generally observed in the region of 3000–2900 cm^{-1}, while the CH_2 symmetric stretch appears in the region 2900–2800 cm^{-1} (Sajan *et al.*, 2004; Balachandran & Parimala, 2012). In this study, the asymmetric stretching vibration of CH_2 group was calculated at 3007 and 2990 cm^{-1} while the symmetric stretching vibration was predicted at 2947 and 2918 cm^{-1}. The deformation was predicted at 1489 and 1468 cm^{-1}. Wagging, twisting and rocking vibrations were predicted below 1390 cm^{-1} as shown in the Table 2. The mixed SC stretching vibration was calculated at 906, 685 and 429 cm^{-1}. CC stretching was predicted at 981 cm^{-1}.

Pyrimidine ring (R2) vibrations

The CH stretching was predicted at 3071 cm^{-1}. The in-plane and out-of-plane bending vibration of this group were predicted at 1210 and 846 cm^{-1}, respectively. The most of the characteristic features of the carboxylic group are observed usually in the region 1700-1800 cm^{-1} (Banwell & McCash, 1994). In this study, C=O stretching was predicted at 1705 cm^{-1} which has very strong intensity of 665 arb. units (i.e., km/mole) in the IR spectrum and medium intensity of 40 units in the Raman spectrum. The in-plane bending related to this group modes vibration was calculated at 631 cm^{-1}.

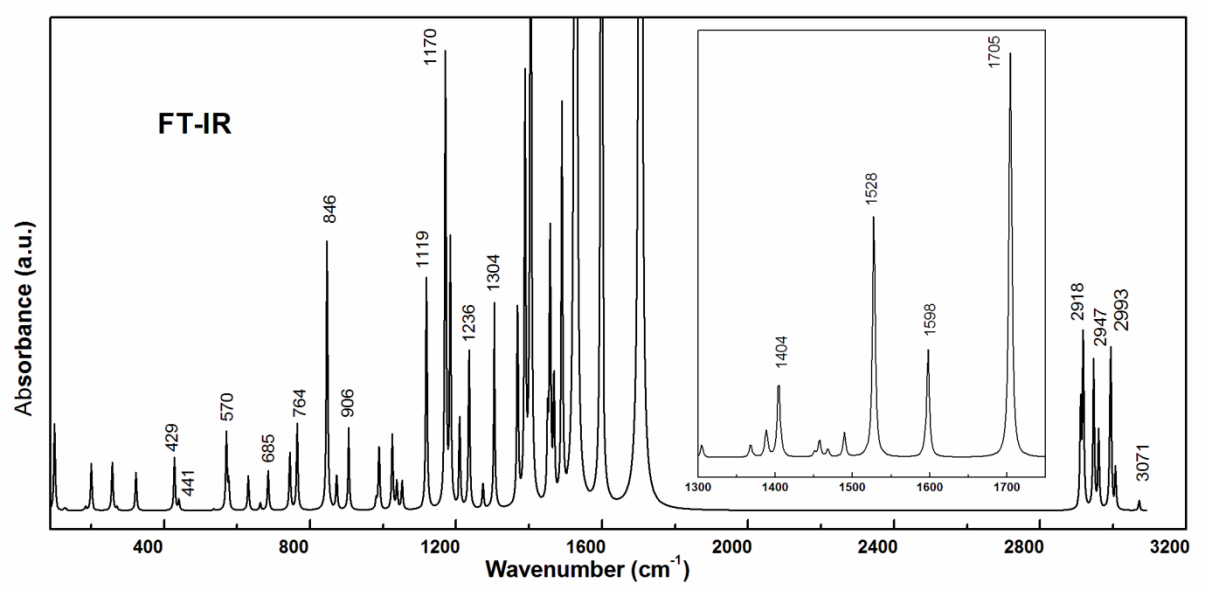

Fig. 5. Calculated FT-IR spectra between the ranges 100-3200 cm^{-1}(frequency ranges 1300-1800 cm^{-1} with high absorbance is given in the inset section). Absorbances of selected characteristic modes are assigned.

C=C ring stretching was predicted at 1598 cm^{-1} with strong intensity in the IR spectrum and weak intensity in the Raman spectrum. N=C stretching was calculated at 1528 cm^{-1}, which has very strong intensity in the IR spectrum (407 km/mole) and medium intensity in the Raman spectrum (67 km/mole). The mixed CC stretching was predicted at 1119 cm^{-1}. Similarly, the NC stretching vibration was predicted at 988 cm^{-1}. The highly mixed ring puckering, deformation, torsion were predicted at 745,741 and 200 cm^{-1}, respectively.

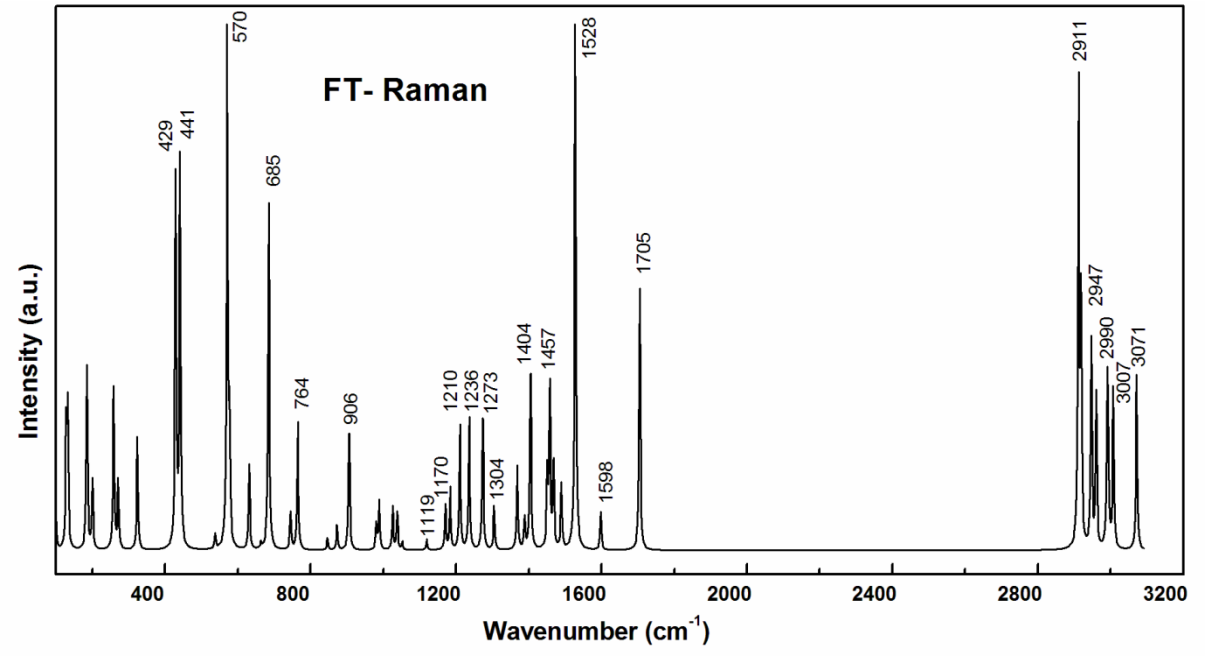

Fig. 6. Calculated FT- Raman spectra between the ranges 100-3200 cm^{-1} (intensity of selected characteristic modes are assigned).

CONCLUSION

We have mainly concentrated to study the wavenumber calculations theoretically. All the assigned 51 modes of vibration are both IR and Raman active. The MEP mapping gives the size, shape, charge density distribution and sites of chemical reactivity of the title molecule which would be a good starting point for studying the detailed potential surface of the molecule. From the HOMO-LUMO plot it is clear that the charge accumulation mainly takes place from HOMO to LUMO both in the gaseous and solvent phases. The gap energy between these two frontier energy levels 5.21 eV (gaseous phase) indicates the high stability of the molecule.

ACKNOWLEDGEMENTS

BD Joshi would like to thank Brazilian National Council of Scientific and Technological Development (CNPq) and TWAS, the academy of sciences for the developing world for the financial support (CNPq-TWAS Post-Doc fellowship-2014/190175/2013-3/FR number: 3240279899) to study Post-Doc at "Universidate Federal do Ceará, CE, Fortaleza, Brazil".

REFERENCES

Al-Omary, F. A.; Hassan, G. S.; El-Messery, S. M. and El-Subbagh, H. I. (2012). Substituted thiazoles V. Synthesis and antitumor activity of novel thiazolo (2,3-*b*) quinazoline and pyrido (4,3-*d*) thiazolo (3,2-*a*) pyrimidine analogues, *European Journal of Medicinal Chemistry*, **47**: 65–72.

Balachandran, V. and Parimala, K. (2012). Molecular structure, vibrational spectra, NBO analysis, first hyperpolarizability, *Journal of Molecular Structure*, **1007**: 136–145.

Balkan, A.; Uma, S.; Ertan, M. and Wiegrebe, W. (1992). Thiazolo (3,2-α)-pyrimidine derivatives as calcium antagonists, *Pharmazie*, **47:** 687–688.

Banwell, C. N. and McCash, E. M. (1994). *Fundamentals of Molecular Spectroscopy*, (fourth ed.), McGraw-Hill International (UK) Limited.

Becke, A. D. (1993). Density-functional thermochemistry. III. The role of exact exchange, *The Journal of Chemical Physics*, **98**: 5648-5652.

Bradley, J. S.; Guidos, R.; Baragona, S. *et al.* (2007). Anti-infective research and development-problems, challenges, and solutions. *The Lancet Infectious Diseases*, **7** (1): 68–78.

Brown, D. J. (1984). *Comprehensive Heterocyclic Chemistry*, vol. 14 (Edited by A.R. Katritzky and C.W. Rees), Pergamon Press, Oxford, UK.

Cai, D.; Zhang, Z. H.; Chen, Y.; Yan, X. J.; Zou, L. J.; Wang, Y. N. *et al.* (2015). Synthesis, Antibacterial and Antitubercular Activities of Some 5*H*-Thiazolo(3,2-*a*)pyrimidin-5-ones and Sulfonic Acid Derivatives, *Molecules*, **20**: 16419-16434.

Casida, M. E. and Chong, D. P. (1995). *Recent Developments in Density Functional Theory*, vol. 1, World Scientific, Singapore, Pp. 155.

Casida, M. E.; Casida, K. C. and Salahub, D. R. (1998). Excited-state potential energy curves from time-dependent density-functional theory: A cross section of formaldehyde's $^1A_1$ manifold. *International Journal of Quantum Chemistry*, **70**: 933-941.

Chamers, J. M. and Griffiths, P. R. (2002). *Handbook of Vibrational Spectroscopy*, John Wiley and Sons.

Chidangil, S.; Shukla, M. K. and Mishra, P. C. (1998). A Molecular Electrostatic Potential Mapping Study of Some Fluoroquinolone Anti-Bacterial Agents. *Journal of Molecular Modeling*, **4**: 250-258.

Danel, K.; Pedersen, E. B. and Nielsen, C. (1998). Synthesis and anti-HIV-1 activity of novel 2,3-dihydro-7 *H*-thiazolo (3,2-*a*) pyrimidin-7-ones. *Journal of Medicinal Chemistry*, **41**: 191–198.

El-Bayouki, K. A. and Basyouni, W. M. (2010). Thiazolopyrimidines without bridge-head nitrogen: Thiazolo (4,5-*d*) pyrimidines. *Journal of Sulfur Chemistry*, **31**: 551–590.

Elderfield, R. C. (1957). *Heterocyclic Compounds*, vol. 6, John Wiley & Sons, New York, NY, USA.

Flefel, E.; Salama, M.; El-Shahat, M.; El-Hashash, M. and El-Farargy, A. (2007). A novel synthesis of some new pyrimidine and thiazolopyrimidine derivatives for anticancer evaluation. *Phosphorus, Sulfur, and Silicon and the Related Elements*, **182**: 1739–1756.

Frisch, A.; Nielson, A. B. and Holder, A. J. (2009). *Gauss View User Manual, Gaussian Inc*, Pittsburgh, P.A.

Frisch, M. J.; Trucks, G. W.; Schlegel, H. B.; Scuseria, G. E.; Cheeseman, J. R.; Robb, M. A.; *et al.*(2009). GAUSSIAN 09, Revision, Gaussian, Inc., Wallingford, CT.

Geist, J. G.; Lauw, S.; Illarionova, V.; Illarionov, B.; Fischer, M.; Gräwert, T. *et al.* (2010). Thiazolopyrimidine inhibitors of 2-methylerythritol 2,4-cyclodiphosphate synthase (IspF) from mycobacterium tuberculosis and plasmodium falciparum. *Chem Med Chem*, **5**: 1092–1101.

Govindarajan, M.; Karabacak, M.; Suvitha, A. and Periandy, S. (2012). FT-IR, FT-Raman, ab initio, HF and DFT studies, NBO, HOMO–LUMO and electronic structure calculations on 4-chloro-3-nitrotoluene. *Spectrochimica Acta Part A*, **89:** 137– 148.

Guirgis, G. A.; Klaboe, P.; Shen, S.; Powell, D. L.; Gruodis, A.; Aleksa, V. *et al.* (2003). Spectra and structure of silicon-containing compounds. XXXVI-Raman and infrared spectra, conformational stability, *ab initio* calculations and vibrational assignment of ethyldibromosilane. *Journal of Raman Spectroscopy*, **34** (4): 322-336.

Hohenberg, P. and Kohn, W. (1964). Inhomogeneous Electron Gas. *Physical Review B*, **136**: 864-871.

Jachak, M. N.; Avhale, A. B.; Tantak, C. D.; Toche, R. B. and Reidlinger, C. (2005). Friedlander condensation of 5-aminopyrazole-4-carbaldehydes with reactive-methylene ketones: Synthesis of pyrazolo (3,4-b) pyridines. *Journal of Heterocyclic Chemistry*, **42**: 1311-1319.

Jeanneau-Nicolle, E.; Benoit-Guyod, M.; Namil, A. and Leclerc, G. (1992). New thiazolo (3,2-*a*) pyrimidine derivatives, synthesis and structure-activity relationships. *European Journal of Medicinal Chemistry*, **27**: 115–120.

Jha, O.; Yadav, T. K. and Yadav, R. A. (2018). Structural and vibrational study of a neurotransmitter molecule: Dopamine (4-(2-aminoethyl) benzene-1,2-diol), *Spectrochimica Acta A*, **189:** 473–484.

Joshi, B. D.; Srivastava, A.; Tandon, P. and Jain, S. (2011). Molecular structure, vibrational spectra and HOMO, LUMO analysis of yohimbine hydrochloride by density functional theory and *ab initio* Hartree–Fock calculations. *Spectrochimica Acta A*, **82**: 270– 278.

Kumar, A.; Kumar, R.; Gupta, A.; Tandon, P. and D'silva, E. D. (2017). Molecular structure, nonlinear optical studies and spectroscopic analysis of chalcone derivative (2E)-3-(4-(methylsulfanyl) phenyl)-1-(3-bromophenyl) prop-2-en-1-one by DFT calculations. *Journal of Molecular Structure*, **1150:** 166-178.

Lee, C.; Yang, W. and Parr, R. G. (1998). Development of the Colic-Salvetti Correlation-Energy Formula into a Functional of the Electron Density. *Physical Review B*, **37**: 785-789.

Martin, J. M. L. and Van Aslenoy, C. (1995). Gar2ped. University of Antwerp.

Mishra, R.; Srivastava, A.; Tandon, P. and Jain, S. (2015). Spectroscopic and quantum chemical analysis of a natural product – Hayatin hydrochloride. *Journal of Mololecular Structure*, **1093**: 101–112.

Mohamed, S. F.; Flefel, E. M.; Amr, A. E. G. E. and El-Shafy, D. N. A. (2010). Anti-HSV-1 activity and mechanism of action of some new synthesized substituted pyrimidine, thiopyrimidine and thiazolopyrimidine derivatives. *European Journal of Medicinal Chemistry*, **45**: 1494–1501.

Nagarajaiah, H.; Khazi, I. and Begum, N. S. (2012). Synthesis, characterization and biological evaluation of thiazolopyrimidine derivatives. *Journal of Chemical Sciences*, **124**: 847–855.

Pan, B.; Huang, R.; Zheng, L.; Chen, C.; Han, S.; Qu, D. *et al.* (2011). Thiazolidione derivatives as novel antibiofilm agents: Design, synthesis, biological evaluation, and structure-activity relationships. *European Journal of Medicinal Chemistry*, **46**: 819–824.

Panlilio, A. L.; Culver, D. H.; Gaynes, R. P. *et al.* (1992). Methicillinresistant staphylococcus aureus in U.S. hospitals, 1975–1991. *Infection Control and Hospital Epidemiology*, **13** (10): 582–586.

Park, H. R.; Kim, J.; Kim, T.; Jo, S.; Yeom, M.; Moon, B. *et al.* (2013). Oxazolopyridines and thiazolopyridines as monoamine oxidase B inhibitors for the treatment of Parkinson's

disease. *Bioorganic & Medicinal Chemistry*, **21**: 5480–5487.

Parr, R. G. and Yang, W. (1989). *Density Functional Theory of Atoms and Molecules*, Oxford, New York.

Perepichka, D. F. and Bryce, M. R. (2005). Molecules with Exceptionally Small HOMO–LUMO Gaps. *Angewandte Chemie International Edition*, **44**: 5370–5373.

Petersson, G. A. and Allaham, M. A. (1991). A Complete Basis Set Model Chemistry. II Open- Shell Systems and the Total Energies of the First-Row Atoms. *The Journal of Chemical Physics*, 9**4**: 6081-6090.

Polavarapu, P. L. (1990). *Ab initio* vibrational Raman and Raman optical activity spectra. *The Journal of Physical Chemistry*, **94(21)**: 8106-8112.

Pulay, P.; Fogarasi, G.; Ponger, G.; Boggs, J. E. and Vargha, A. (1983). Combination of theoretical *ab initio* and experimental information to obtain reliable harmonic force constants. Scaled Quantum Mechanical (SQM) force fields for glyoxal, acrolein, butadiene, formaldehyde, and ethylene. *Journal of American Chemical Society*, **105** (24): 7037-7047.

Sajan, D.; Binoy, J.; Pradeep, B.; Venkata Krishna, K.; Kartha, V. B., Joe, I. H. *et al.* (2004). NIR-FT Raman and infrared spectra and ab initio computations of glycinium oxalate. *Spectrochimica Acta A*, **60**: 173–180.

Singh, R. N.; Kumar, A.; Tiwari, R. K.; Rawat, P.; Verma, D. and Baboo, V. (2012). Synthesis, molecular structure and spectral analysis of ethyl 4-formyl-3,5-dimethyl-1H-pyrrole-2-carboxylate thiosemicarbazone: A combined DFT and AIM approach. *Journal of Molecular Structure*, **1016:** 97–108.

Srivastava, A.; Mishra, S.; Tandon, P.; Patel, S.; Ayala, A. P.; Bansal, A. K. *et al.* (2010). Molecular structure and vibrational spectroscopic analysis of an antiplatelet drug, clopidogrel hydrogen sulphate (form 2) – A combined experimental and quantum chemical approach. *Journal of Molecular Structure*, **964:** 88–96.

Tozkoparan, B.; Ertan, M.; Kelicen, P. and Demirdamar, R. (1999). Synthesis and anti-inflammatory activities of some thiazolo (3,2-*a*) pyrimidine derivatives. *Farmaco*, **54**: 588–593.

Yoshida, H.; Takeda, K.; Okamura, J.; Ehara, A. and Matsurra, H. (2002*).* A new approach to vibrational analysis of large molecules by density functional theory: wavenumber-linear scaling method. *The Journal of Physical Chemistry A*, **106** (14): 3580-3586.

Zhurko, G. A. and Zhurko, D. A. (2005). *Chemcraft - 64 bit, US version (Online)* <*http://www.chemcraftprog.com*>.